

Time-wavelength optical sampling spectroscopy based on dynamic laser cavity tuning

SRIKAMAL J. SOUNDARARAJAN,¹ LIN YANG,¹ SHUQIN ZHANG,^{1,2} HEMANG JANI,¹ LINGZE DUAN^{1,*}

¹Department of Physics, the University of Alabama in Huntsville, Huntsville, AL 35899, USA

²Institute of Optical & Electronic Technology, China Jiliang University, Hangzhou, P. R. China

*Corresponding author: ld0003@uah.edu

Received XX Month XXXX; revised XX Month, XXXX; accepted XX Month XXXX; posted XX Month XXXX (Doc. ID XXXXX); published XX Month XXXX

Time-wavelength optical sampling (TWOS) is proposed here as a scheme that leverages the advantages of both wavelength-time mapping and ultrafast optical sampling to achieve real-time spectral measurement with simple configurations and slow photodetectors. As a proof of concept, a TWOS spectrometer based on dynamic optical sampling by laser cavity tuning is developed. Real-time absorption spectroscopy with a 0.3-nm spectral resolution and a 60-nm total spectral range (laser-limited) is demonstrated at an 150-Hz updating rate. Theoretical analysis and practical limiting factors are discussed in detail. Potential applications of TWOS include spectroscopy, imaging, metrology, and optical sensing. © 2018 Optical Society of America

OCIS codes: (260.2030) Dispersion; (320.1590) Chirping; (300.6500) Spectroscopy, time-resolved; (300.1030) Absorption; (320.7150) Ultrafast spectroscopy; (120.6200) Spectrometers and spectroscopic instrumentation.

<http://dx.doi.org/10.1364/AO.99.099999>

1. INTRODUCTION

Wavelength-time mapping (WTM) is a well-established technique, which converts the spectral components of an ultrafast optical signal into a temporal sequence via linear dispersion. It has been associated with a variety of names, including, for example, frequency-to-time mapping [1], time lens [2], real-time Fourier transformation [3], and dispersive Fourier transformation [4], and has been used in a number of contexts, such as real-time spectroscopy [5-7], arbitrary waveform generation [8,9], analog-to-digital conversion [10,11], and fast imaging [12]. This wide range of applications underscores the ubiquitous importance of time-wavelength transformation in the general field of photonics.

In a standard WTM scheme, a fast photodetector is used to probe the dispersively stretched pulse and convert it into a sequence of power readings that represent the spectral profile of the original pulse [3-12]. This method has proved to be both schematically simple and effective, with the most notable feature being its single-shot capability [13]. However, direct photo-detection does not come without drawbacks. First of all, it puts stringent requirements on the detection system because the speeds of the photodetector and the subsequent electronics dictate the spectral resolution [4]. As a result, photodetectors with tens-of-GHz bandwidths and wideband electronic digitizers (e.g., sampling oscilloscopes) are often required in such schemes [5,10].

Moreover, there is a fundamental trade-off between spectral resolution and signal-to-noise ratio (SNR) since large dispersion often coincides with high optical loss [13]. This problem can be mitigated by employing distributed Raman amplification in dispersive fibers [7,13]. But such additions are often accompanied with significantly increased cost and system complexity.

Meanwhile, recent advance in high-repetition-rate ultrafast optical sources has made it possible to make a variety types of “real-time” measurements with periodical pulse trains. The foundation of these techniques is optical sampling [14,15], which uses optical gating instead of electronic gating to achieve superior temporal resolutions. With today’s femtosecond laser sources, optical pulses with durations comparable to or even shorter than 100 fs can be routinely generated at rates well exceeding 100 MHz [16]. As a result, optical sampling can easily surpass its electronic counterpart in terms of temporal resolution by 2–3 orders of magnitude. Moreover, since optical sampling photo-detect cross-correlation instead of the optical signal itself, it does not require high-speed detection systems and its signal-to-noise ratio is less susceptible to low signal powers, two aspects especially relevant in the current context [17]. Because of these unique features, ultrafast optical sampling (UOS) has gained tremendous interest in recent years and has been applied to a number of fields including sensing, metrology, spectroscopy and imaging [18-30]. Several techniques have been developed to leverage the high pulse repetition rates to achieve real-time measurements, including asynchronous optical

sampling (ASOPS) [18-21], dual-comb spectroscopy [22-24], and dynamic optical sampling by laser cavity tuning (OSCAT) [25-30]. They have demonstrated the feasibility or potential to reach a measurement updating rate well above 1 kHz, and in some cases, into the megahertz range [24].

Here, we propose a new scheme, which combines key aspects of WTM and UOS to address the aforementioned shortcomings of conventional WTM schemes while maintaining the capability of making real-time measurement. We call it time-wavelength optical sampling (TWOS). In TWOS, direct photodetection and electronic sampling are replaced with optical sampling and crosscorrelation measurement. As a result, fast photodetectors and electronics are no longer necessary and the tradeoff between spectral resolution and SNR is mitigated because of the significantly shorter optical sampling signals. Meanwhile, by introducing WTM into an UOS scheme, some of the problems associated with standard UOS are also addressed. For example, TWOS requires sampling the *power* profile of the time-stretched pulse instead of the *field* profile. This alleviates the need for fringe-level coherence between the signal pulse and the gating pulse, something that is typically required in standard UOS schemes [18-30]. The combination of the above features leads to a very simple and cost-effective scheme, which, albeit not single shot, can nevertheless achieve real-time updating without the need for high-speed detectors and digitizers. In the following, we present a proof-of-principle demonstration of TWOS in absorption spectroscopy. It should be kept in mind, however, that the general idea of TWOS is applicable under a wide range of contexts.

2. PRINCIPLE OF OPERATION

The operating principle of TWOS is illustrated in Fig. 1. The system consists of two parts: *i*) a linear dispersive element (e.g., optical fiber) performs WTM by stretching the signal pulses, as shown in Fig. 1(a); *ii*) a tunable interferometer performs the sampling operation on the time-stretched pulses to generate a cross-correlation output, as conceptually depicted in Fig. 1(b). The relative delay scan between the signal pulse train and the sampling pulse train can be accomplished by something as simple as a tunable optical delay line. However, for *in situ* applications that demand quick update rates, conventional mechanical optical delays may not be able to meet the requirements in both scan rate and scan depth simultaneously [27].

In the current research, this problem is addressed by employing a dynamic OSCAT technique we have developed over the last few years [17,27]. In this scheme, a rapid scan of pulse repetition rate is generated by modulating the cavity length of the ultrafast mode-locked laser, which is accomplished by driving an intracavity piezoelectric (PZT) actuator with a periodically changing voltage. This rep-rate scan is then converted into a scan of relative pulse delay via an interferometer with highly imbalanced arm lengths. It has been shown that the maximum pulse delay variation in terms of free-space length, denoted as Δl_d here, is related to the cavity length variation ΔL_c through [27]

$$\Delta l_d = (\Delta l_i / L_{c0}) \Delta L_c, \quad (1)$$

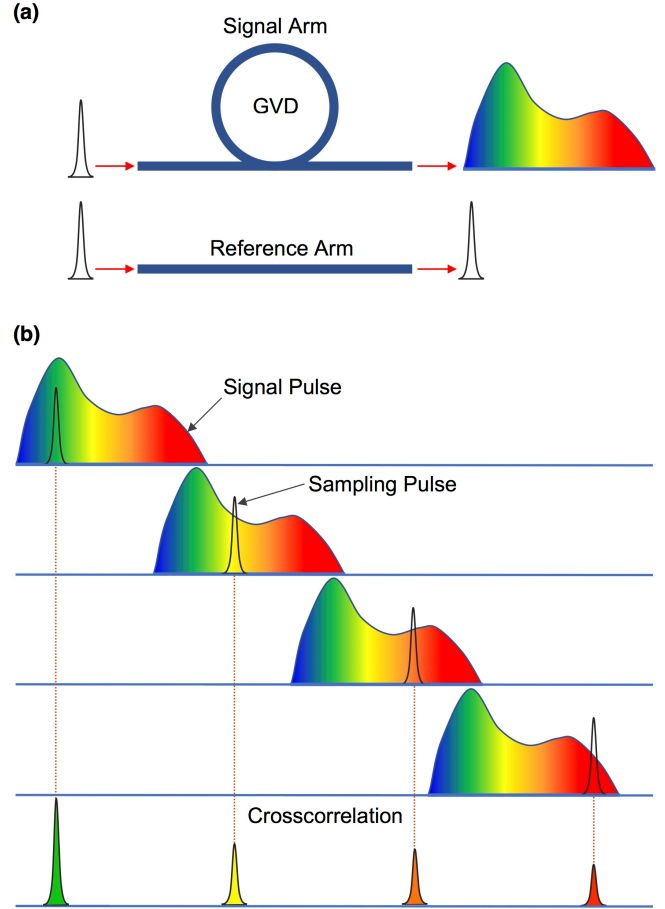


Fig. 1. The operating principle of TWOS spectroscopy: (a) dispersive wavelength-to-time mapping creates the time-stretched signal pulses; (b) optical sampling on the signal pulses generates crosscorrelations proportional to the spectral profile.

where Δl_i is the interferometer arm-length difference and L_{c0} is the nominal laser cavity length. Since L_{c0} is on the order of 0.1 m for typical mode-locked fiber lasers and Δl_i can be as large as 1–10 km with fiber interferometers, the factor inside the parentheses in (1) is typically $\sim 10^4$ – 10^5 , which means a micron-scale cavity length tuning can lead to a centimeter-scale scan of relative pulse delay. Such a dramatic gain in length scale allows the use of wideband, small-displacement actuators such as PZT actuators to generate rapid scan of pulse delay with large scan depths. For example, kHz-scale scan rate and cm-scale scan depth have been demonstrated with dynamic OSCAT [27], while intracavity PZT actuators with bandwidths as large as 200 kHz have been realized experimentally [31].

It should be pointed out that dynamic OSCAT in fact suits especially well with TWOS because the long arm of the fiber interferometer can play the dual-function of both pulse stretching and pulse delay. The result is a very simple system configuration as shown in Fig. 2(a).

In the current context of TWOS spectroscopy, it is instructive to take a close look at the various factors affecting spectral resolution. First and foremost, the time-wavelength mapping ratio is given approximately by [4]

$$\frac{\Delta\lambda}{\Delta\tau} = \frac{1}{|D|l}, \quad (2)$$

where $\Delta\lambda$ is the bandwidth of the ultrafast laser; $\Delta\tau$ is the duration of the stretched pulse; D and l are the group-velocity dispersion (GVD) parameter and the length of the pulse stretching fiber, respectively. Here, the mapping from $\Delta\lambda$ to $\Delta\tau$ is considered as linear and higher-order dispersion terms are neglected. This proves to be a very good approximation as shown by experiment later. Next, we examine the sampling process. According to Fig. 1(b), the sampling pulses scan across the wavelength-mapped signal pulses like a “sliding window”. The minimum resolvable temporal width is determined by both the “window width” and the progression step of the sliding window. The former is simply the full width at half maximum of the sampling pulses, denoted as $\Delta\tau_{FWHM}$. The latter can be estimated using the dynamic OSCAT formula developed in [27],

$$\Delta T_d(t) = \delta T_0 + \frac{\Delta f_R \Delta T_0}{f_{R0}} \sin \left[2\pi f_m \left(t + \frac{\Delta T_0}{2} \right) \right], \quad (3)$$

where $\Delta T_d(t)$ is the relative time delay between signal and sampling pulses, δT_0 is a time offset, f_m is the intracavity modulation frequency, f_{R0} is nominal pulse repetition rate, Δf_R is the maximum deviation of pulse repetition rate due to the intracavity modulation, and ΔT_0 is time delay caused by the arm-length difference of the interferometer. A sinusoidal modulation is assumed here and the modulation frequency is taken to be much lower than the pulse repetition rate. Taking the derivative of (3) yields the changing rate of relative pulse delay

$$\frac{d\Delta T_d}{dt} = 2\pi f_m \frac{\Delta f_R \Delta T_0}{f_{R0}} \cos \left[2\pi f_m \left(t + \frac{\Delta T_0}{2} \right) \right]. \quad (4)$$

What we are interested in here is the maximum change of relative pulse delay over the time between two consecutive pulses, denoted as $\delta\tau_{OSCAT}$. This can be found by multiplying the term before cosine with $1/f_{R0}$, which yields

$$\delta\tau_{OSCAT} = 2\pi f_m \frac{\Delta f_R \Delta T_0}{f_{R0}^2}. \quad (5)$$

The overall temporal resolution of the sampling pulse train is set by the greater factor between pulse width and pulse advancement step:

$$\delta\tau_{smp} = \max(\delta\tau_{FWHM}, \delta\tau_{OSCAT}). \quad (6)$$

Combining (2) and (6), the overall TWOS spectral resolution is given by

$$\delta\lambda_{TWOS} = \frac{\delta\tau_{smp}}{|D|l}. \quad (7)$$

Equation (7) indicates that the minimum resolvable wavelength of a TWOS spectrometer is proportional to the temporal resolution of the sampling pulse train and inversely proportional to the total GVD experienced by the signal pulse train.

Another important parameter for spectrometers is total spectral range. In an OSCAT-based TWOS system, this is determined by the total time-delay variation set forth by OSCAT scan as well as the

total GVD involved in pulse stretching. Combining (2) and (3), it is straightforward to find out that total spectral range can be written as

$$\Delta\lambda_{SR} = 2 \frac{\Delta f_R \Delta T_0}{f_{R0} |D|l}, \quad (8)$$

where the factor 2 stems from the use of peak-to-peak time-delay variation in (3).

3. EXPERIMENTAL SETUP

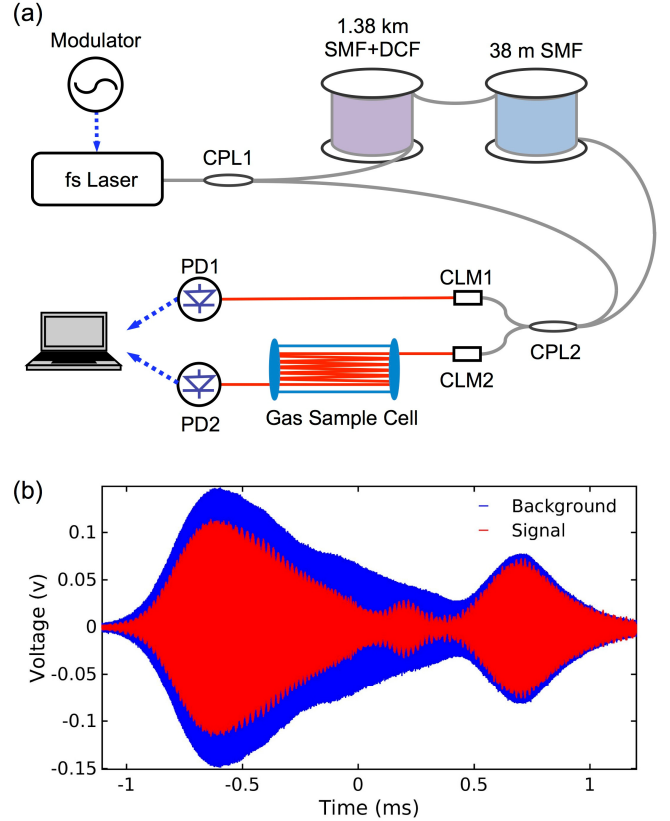


Fig. 2. An OSCAT-based TWOS spectrometer: (a) system schematics, CLM: fiber collimator, CPL: fiber coupler, DCF: dispersion compensating fiber, PD: photodetector, SMF: single-mode fiber; (b) typical time-domain signal (inner, red) and background (outer, blue) cross-correlation traces.

To demonstrate the principle of TWOS spectroscopy, we have built a TWOS spectrometer based on our OSCAT system [29]. Fig. 2(a) shows the system schematics. The light source is a femtosecond mode-locked fiber laser (Menlo Systems M-Comb), operating at a center wavelength of 1540 nm with a repetition rate of 250 MHz. An intracavity PZT actuator attached on one of the cavity mirrors is driven by an external modulator. Under a sinusoidal modulation, the peak-to-peak variation of repetition rate is about 3.55 KHz. The laser output is coupled into a Mach-Zehnder interferometer (MZI) via fiber coupler CPL1. Most of the power (about 30 mW) is directed into the long signal arm, which consists of 1.24-km single-mode fiber (SMF-28) and 142-m dispersion compensating fiber (DCF). These lengths of fibers are chosen so that the positive and negative GVDs are optimally cancelled and the signal pulses are

fully recompressed at the end of the 1.38-km fiber link. An extra 38-m SMF is then added to the signal arm for the purpose of pulse stretching. With an estimated GVD of about 18 ps/(nm km), the time-stretched signal pulses have an approximate width of 30 ps. Meanwhile, a small portion of the laser output (about 3 mW) is routed through the short reference arm to provide the sampling pulses. This short arm is 5 m in length and is made of both SMF and DCF for GVD management. The final sampling pulse width is about 200 fs. The two pulse trains are mixed at fiber coupler CPL2 and split into two free-space paths via fiber collimators CLM1 and CLM2. One of these beams is directly focused onto a photodetector (PD1) to produce the background crosscorrelation trace, which is essentially the spectrum of the laser free of sample absorption. The other beam goes through an atomic gas cell via a multi-pass system before impinging on a second and identical photodetector (PD2). The generated crosscorrelation traces carry imprints of the atomic absorption spectrum. A typical pair of background (blue) and signal (red) crosscorrelation traces is shown in Fig. 2(b). The signal trace bears apparent absorption patterns. These patterns can be extracted out of the background using proper computer algorithms. The resulted time-domain traces also need to be mapped back to the frequency domain. In practice, this is done by calibrating the TWOS spectrometer against certain spectral features whose wavelengths can be precisely measured through other means (e.g., spectrum analyzers). The rate of the intracavity scan is controlled by the modulation frequency applied on the PZT. Scanning rates as fast as 200 Hz have been successfully tested on our current setup, as evident from the time scale of Fig. 2(b).

4. EXPERIMENTAL RESULTS

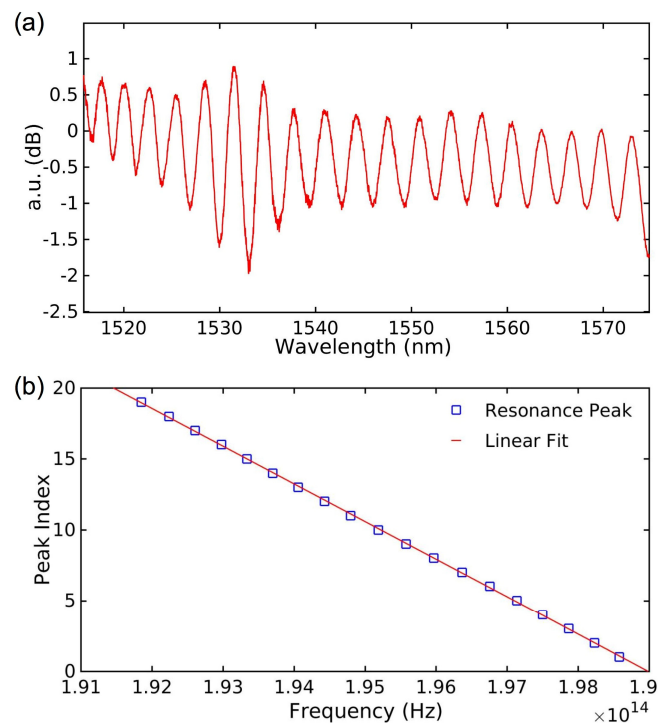


Fig. 3. Reflective spectrum from a Fabry-Perot etalon measured by the TWOS spectrometer. (a) Periodic resonance peaks are seen over a 60-nm span. (b) The measured resonance frequencies display an excellent linearity, indicating a good linear dispersive mapping.

Before the TWOS spectrometer can be used on atomic samples, some of its key properties, such as effective spectral width and the linearity of WTM, need to be characterized. This has been done by using a Fabry-Perot etalon (FPE) as the sample and measuring the reflected spectrum with the spectrometer. The FPE is made of a glass substrate of 200- μm thickness, with 35-nm layers of Cr coating sputtered on both sides. It is placed directly against the collimator CLM2 and a fiber circulator is inserted immediately before CLM2 to route the reflected pulse trains to PD2. Fig. 3(a) shows the measured spectrum upon proper data extraction and calibration. Periodic resonance peaks are clearly resolved from 1515 nm to 1575 nm. The 482-GHz measured free-spectral range agrees well with the 200- μm etalon thickness. The frequencies of these resonance peaks are found to follow a highly linear distribution, as shown in Fig. 3(b). This indicates excellent linear mapping between wavelength and time across the entire 60-nm effective wavelength span.

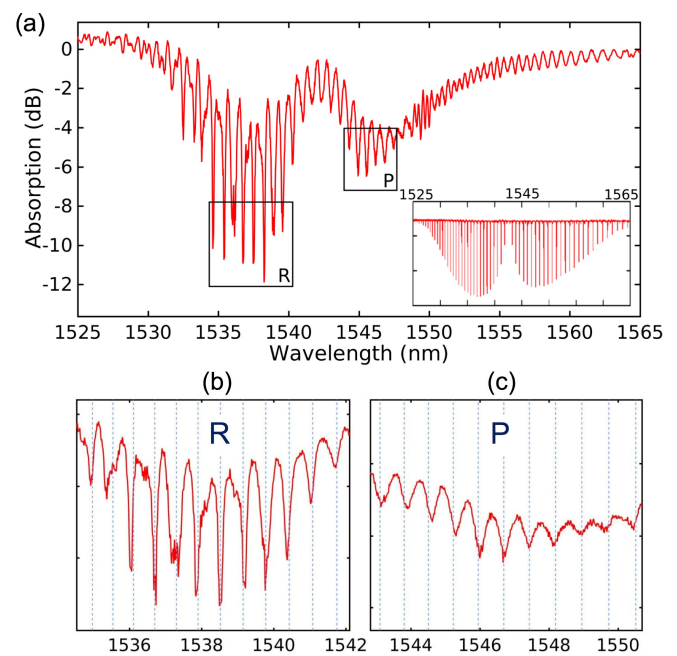


Fig. 4. Absorption spectrum of HCN (at 330 Torr) measured by the TWOS spectrometer. (a) The overall spectrum showing both the R and P branches (Inset: standard HCN absorption spectrum). (b) and (c) Zoom-in view of R and P branches, respectively, as compared to the HITRAN absorption lines.

Next, we use TWOS spectroscopy to analyze atomic samples. Fig. 4 summarizes the results based on a HCN gas sample at 330 Torr in a 5-cm gas cell. Fig. 4(a) is absorption spectrum resulted from a broadband scan (1525 nm – 1565 nm). The scan is performed at a rate of 150 Hz, meaning it requires less than 7 ms to generate a full spectrogram. The spectrogram clearly reveals the R and P branches of HCN, whose HITRAN spectrum is shown in Fig. 4(a) inset. The close similarity between the measured spectrum and the documented spectrum indicates the effectiveness of our TWOS spectrometer. To further verify the accuracy of the measured spectrum, finer scans are taken around the center regions of both branches (indicated in Fig. 4(a) with dark squares). The resulted spectrograms are shown in Fig. 4(b) and (c). In both cases, the measured absorption peaks are plotted

against the grid formed by HITRAN absorption lines. The agreement is found to be very good. It should be noted that the apparent overlapping between adjacent spectral lines in the spectrograms is primarily due to the high pressure (330 Torr) of the gas cell used in the experiment.

5. DISCUSSIONS AND CONCLUSION

We now examine the factors that limit the performance of our current TWOS spectrometer.

First, according to (7), the spectral resolution is determined by the total GVD of the pulse-stretching fiber D/l as well as the gating window width $\delta\tau_{\text{Smp}}$. The latter is the greater one between sampling pulse width $\delta\tau_{\text{FWHM}}$ and OSCAT pulse-delay advancement $\delta\tau_{\text{OSCAT}}$. For the current system, $\delta\tau_{\text{FWHM}} \approx 200$ fs, and $\delta\tau_{\text{OSCAT}}$ can be estimated based on (5) and relevant system parameters, $f_m = 150$ Hz, $f_{R0} = 250$ MHz, $\Delta f_R = 1.78$ kHz, and $\Delta T_0 \approx 6.9$ μ s, which yield $\delta\tau_{\text{OSCAT}} \approx 0.2$ fs. Apparently, $\delta\tau_{\text{FWHM}}$ is the dominating factor. With 38-m pulse-stretching fiber at a nominal GVD of 18 ps/(nm km), the wavelength resolution $\delta\lambda_{\text{TWOS}}$ is estimated to be approximately 0.3 nm, or 38 GHz. This is about one order of magnitude smaller than the common commercial grating-based spectrometers in this wavelength range and about one order of magnitude larger than the best result based on the conventional WTM scheme [7]. For a proof-of-principle demonstration, we believe this result shows the potential of TWOS spectroscopy. The current spectral resolution is achieved with a very simple system and a mere 38-m pulse stretching fiber. This fiber length is primarily restricted by our wavelength calibration method, but there is no fundamental limit preventing the fiber length, or equivalently, the total GVD, to be much greater. In fact, pulse-stretching fibers of kilometer scale or longer have been routinely used in WTM schemes [5]. It is therefore conceivable that a spectral resolution one- to two-orders-of-magnitude better can be realized with TWOS spectroscopy.

Next, the maximum spectral coverage of the spectrometer is given by (8). Using the aforementioned system parameters, $\Delta\lambda_{\text{SR}}$ is found to be approximately 140 nm. The current system, however, is limited by the 60-nm bandwidth of the mode-locked laser. With nonlinear spectral broadening, the restriction set forth by laser spectral range can be easily overcome. Further expanding the spectral coverage of the OSCAT system would require increasing the ratio of $\Delta f_R/f_{R0}$ and the value of ΔT_0 . Since $\Delta f_R/f_{R0} = \Delta L_c/L_{c0}$, the first requirement effectively calls for larger intracavity modulation relative to the nominal cavity length. This can be done by opting for mode-locked lasers with higher repetition rates (hence smaller L_{c0}). It should be noted here that mode-locked lasers with GHz repetition rates are widely available nowadays [16]. Meanwhile, increasing the value of ΔT_0 simply requires extending the length of the long arm in the OSCAT system, which appears to be much easier to accomplish. For example, a 10-km long arm in our current OSCAT system in principle could expand the spectral range of the spectrometer to about 1000 nm.

Finally, it should be pointed out that the work reported here is only a case study of TWOS and the concept of TWOS is much more generic. Its application is not restricted to spectroscopy, nor does its implementation have to involve OSCAT. One can easily envision combining TWOS with other ultrafast optical sampling techniques such as ASOPS and applying it to a breadth of fields ranging from imaging to metrology to optical sensing, etc.

In conclusion, the concept of TWOS is proposed here as an alternative to conventional WTM schemes based on direct photodetection. When combined with emerging ultrafast optical-sampling techniques such as ASOPS and OSCAT, TWOS has the potential to realize real-time measurement with high temporal resolution without the need for high-speed photo-detectors and complicated amplification systems. OSCAT-based TWOS spectroscopy has been theoretically analyzed and experimentally demonstrated. A spectral resolution of 0.3 nm and a total spectral range of 60 nm (laser-limited) have been demonstrated near 1540 nm with a very simple system including only 38-m pulse-stretching fiber. Spectrograms obtained at updating rates as fast as 150 Hz with an HCN gas sample show excellent agreement with standard results. The work could serve as a proof-of-principle study for many future applications of TWOS.

Funding Information. National Science Foundation (NSF) (ECCS-1254902 and ECCS-1606836).

Acknowledgment. We thank the Center for Applied Optics and Nano and Micro Devices Center for their assistance throughout the research.

References

1. V. Torres-Company, D. E. Leaird, and A. M. Weiner, "Dispersion requirements in coherent frequency-to-time mapping," *Opt. Express* **19**, 24718 (2011).
2. B. H. Kolner and M. Nazarathy, "Temporal imaging with a time lens," *Opt. Lett.* **14**, 630 (1989).
3. T. Jansson, "Real-time Fourier transformation in dispersive optical fibers," *Opt. Lett.* **8**, 232 (1983).
4. K. Goda and B. Jalali, "Dispersive Fourier transformation for fast continuous single-shot measurement," *Nat. Photon.* **7**, 102 (2013).
5. J. Chou, Y. Han, B. Jalali, "Time-wavelength spectroscopy for chemical sensing," *IEEE Photon. Tech. Lett.* **16**, 1140 (2004).
6. J. Hult, R. S. Watt, and C. F. Kaminski, "High bandwidth absorption spectroscopy with a dispersed supercontinuum source," *Opt. Express* **15**, 11385 (2007).
7. J. Chou, D. R. Solli, and B. Jalali, "Real-time spectroscopy with subgigahertz resolution using amplified dispersive Fourier transformation," *Appl. Phys. Lett.* **92**, 111102 (2008).
8. C. Wang and J. Yao, "Simultaneous optical spectral shaping and wavelength-to-time mapping for photonic microwave arbitrary waveform generation," *IEEE Photon. Tech. Lett.* **21**, 793 (2009).
9. A. Dezfooliyani and A. M. Weiner, "Photonic synthesis of high fidelity microwave arbitrary waveforms using near field frequency to time mapping," *Opt. Express* **21**, 22974 (2013).
10. A. S. Bhushan, F. Coppinger, and B. Jalali, "Time-stretched analog-to-digital conversion," *Electron. Lett.* **34**, 839 (1998).
11. A. M. Fard, B. Buckley, S. Zlatanovic, C. S. Bres, S. Radic, and B. Jalali, "All-optical time-stretch digitizer," *Appl. Phys. Lett.* **101**, 051113 (2012).
12. K. Goda, K. K. Tsia, and B. Jalali, "Serial time-encoded amplified imaging for real-time observation of fast dynamic phenomena," *Nature* **458**, 1145 (2009).
13. D. R. Solli, J. Chou, and B. Jalali, "Amplified wavelength-time transformation for real-time spectroscopy," *Nat. Photon.* **2**, 48 (2007).
14. C. Dorrer, "High-speed measurements for optical telecommunication systems," *IEEE J. Sel. Topics Quantum Electron.* **12**, 843 (2006).
15. G. Berrettini, A. Bogoni, F. Fresi, G. Meloni, and L. Poti, "Evolution of optical sampling," in *Advances in Lasers and Electro Optics*, N. Costa and A. Cartaxo, eds. (INTECH, 2010), pp. 289-314.

16. U. Keller, "Recent developments in compact ultrafast lasers," *Nature* **424**, 831 (2003).
17. L. Duan and L. Yang, "Ultrafast optical sampling finds applications in precision measurement," *J. Sci. Ind. Metrol.* **1**, 1 (2016).
18. C. Janke, M. Först, M. Nagel, and H. Kurz, "Asynchronous optical sampling for high-speed characterization of integrated resonant terahertz sensors," *Opt. Lett.* **30**, 1405 (2005).
19. A. Bartels, R. Cerna, C. Kistner, A. Thoma, F. Hudert, C. Janke, and T. Dekorsy, "Ultrafast time-domain spectroscopy based on high-speed asynchronous optical sampling," *Rev. Sci. Instrum.* **78**, 035107 (2007).
20. T. Liu, N. R. Newbury, and I. Coddington, "Sub-micron absolute distance measurements in sub-millisecond times with dual free-running femtosecond Er fiber-lasers," *Opt. Express* **19**, 1 (2011).
21. S. Kray, F. Spöler, M. Först, and H. Kurz, "Dual femtosecond laser multiheterodyne optical coherence tomography," *Opt. Lett.* **33**, 2092 (2008).
22. S. Schiller, "Spectrometry with frequency combs," *Opt. Lett.* **27**, 766 (2002).
23. B. Bernhardt, E. Sorokin, P. Jacquet, R. Thon, T. Becker, I. T. Sorokina, N. Picqué, T. W. Hänsch, "Mid-infrared dual-comb spectroscopy with 2.4 μm Cr^{2+} :ZnSe femtosecond lasers," *Appl. Phys. B* **100**, 3 (2010).
24. I. Coddington, N. Newbury, and W. Swann, "Dual-comb spectroscopy," *Optica* **3**, 414 (2016).
25. T. Hochrein, R. Wilk, M. Mei, R. Holzwarth, N. Krumbholz, and M. Koch, "Optical sampling by laser cavity tuning," *Opt. Express* **18**, 1613 (2010).
26. S. Potvin, S. Boudreau, J. Deschênes, and J. Genest, "Fully referenced single-comb interferometry using optical sampling by laser-cavity tuning," *Appl. Opt.* **52**, 248 (2013).
27. L. Yang, J. Nie and L. Duan, "Dynamic optical sampling by cavity tuning and its application in lidar," *Opt. Express* **21**, 3850 (2013).
28. S. Boudreau and J. Genest, "Range-resolved vibrometry using a frequency comb in the OSCAT configuration," *Opt. Express* **22**, 8101 (2014).
29. L. Yang and L. Duan "Depth-resolved imaging based on optical sampling by cavity tuning," *IEEE Photon. Technol. Lett.* **27**, 1761 (2015).
30. K. Lee, J. Lee, Y. Jang, S. Han, H. Jang, Y. Kim and S. Kim, "Fourier-transform spectroscopy using an Er-doped fiber femtosecond laser by sweeping the pulse repetition rate," *Sci. Reports* **5**, 15726 (2015).
31. T.C. Briles, D. C. Yost, A. Cingöz, J. Ye, and T. R. Schibli, "Simple piezoelectric-actuated mirror with 180 kHz servo bandwidth," *Opt. Express* **18**, 9739 (2010).